THE JOURNAL OF BIOLOGICAL CHEMISTRY VOL. 282, NO. 12, pp. 8860–8872, March 23, 2007

Inhibition of Mitochondrial Respiration as a Source of Adaphostin-induced Reactive Oxygen Species and Cytotoxicity*

Received for publication, July 12, 2006 Published, JBC Papers in Press, January 9, 2007, DOI 10.1074/jbc.M611777200

Son B. Le[‡1], M. Katie Hailer[‡], Sarah Buhrow[‡], Qi Wang[§], Karen Flatten[‡], Peter Pediaditakis[¶], Keith C. Bible[‡‖], Lionel D. Lewis[**], Edward A. Sausville[‡‡], Yuan-Ping Pang[§‖], Matthew M. Ames[‡‖], John J. Lemasters[¶2], Ekhson L. Holmuhamedov[¶3], and Scott H. Kaufmann[‡‖3,4]

From the Departments of [‡]Oncology, [§]Physiology and Biomedical Engineering, and [‖]Molecular Pharmacology, Mayo Clinic College of Medicine, Rochester, Minnesota 55905, the [¶]Department of Cell and Developmental Biology, University of North Carolina, Chapel Hill, North Carolina 27599, the [**]Department of Medicine, Dartmouth Medical School, Lebanon, New Hampshire 03756, and the [‡‡]Greenebaum Cancer Center, Baltimore, Maryland 21201

Adaphostin is a dihydroquinone derivative that is undergoing extensive preclinical testing as a potential anticancer drug. Previous studies have suggested that the generation of reactive oxygen species (ROS) plays a critical role in the cytotoxicity of this agent. In this study, we investigated the source of these ROS. Consistent with the known chemical properties of dihydroquinones, adaphostin simultaneously underwent oxidation to the corresponding quinone and generated ROS under aqueous conditions. Interestingly, however, this quinone was not detected in intact cells. Instead, high performance liquid chromatography demonstrated that adaphostin was concentrated by up to 300-fold in cells relative to the extracellular medium and that the highest concentration of adaphostin (3000-fold over extracellular concentrations) was detected in mitochondria. Consistent with a mitochondrial site for adaphostin action, adaphostin-induced ROS production was diminished by >75% in MOLT-4 rho^0 cells, which lack mitochondrial electron transport, relative to parental MOLT-4 cells. In addition, inhibition of oxygen consumption was observed when intact cells were treated with adaphostin. Loading of isolated mitochondria to equivalent adaphostin concentrations caused inhibition of uncoupled oxygen consumption in mitochondria incubated with the complex I substrates pyruvate and malate or the complex II substrate succinate. Further analysis demonstrated that adaphostin had no effect on pyruvate or succinate dehydrogenase activity. Instead, adaphostin inhibited reduced decylubiquinone-induced cytochrome *c* reduction, identifying complex III as the site of inhibition by this agent. Moreover, adaphostin enhanced the production of ROS by succinate-charged mitochondria. Collectively, these observations demonstrate that mitochondrial respiration rather than direct redox cycling of the hydroquinone moiety is a source of adaphostin-induced ROS and identify complex III as a potential target for antineoplastic agents.

Adaphostin (NSC680410) is a dihydroquinone derivative that is undergoing preclinical testing as a potential anti-leukemic drug. Previous studies have demonstrated that this agent is toxic to clinical isolates of chronic myelogenous leukemia but not normal bone marrow progenitors (1, 2). More recently, this agent has been reported to retain activity against imatinib-resistant chronic myelogenous leukemia, including cells expressing Bcr/Abl mutants that are resistant to currently available kinase inhibitors (3). Nonetheless, the anti-leukemic activity of this agent does not depend on the presence of the Bcr/Abl kinase, as selectivity in killing acute myelogenous leukemia (4) and chronic lymphocytic leukemia (5) cells is also observed *in vitro*. Based on these results, there is considerable interest in identifying the mechanism by which adaphostin kills cells.

Previous studies (3–6) have suggested that adaphostin kills target cells through a mechanism that involves up-regulation of reactive oxygen species (ROS).[5] Evidence in support of this view includes increased oxidation of the dyes 5(6)-chloromethyldihydro-2′,7′-dichlorofluorescein (CM-H_2DCF) and dihydroethidium in adaphostin-treated cells, including Bcr/Abl-negative ML-1 and Jurkat cells, as well as the ability of the antioxidants *N*-acetylcysteine (CysNAc), tiron, and Trolox to inhibit the cytotoxicity of adaphostin (4, 6). On the other hand, it has also been recognized that dyes such as 5(6)-chloromethyl-2′,7′-dichlorofluorescein (CM-DCF) are subject to efflux by

* This work was supported in part by National Institutes of Health Grant R01 CA85972, the Mayo Foundation for Education and Research, and the University of Minnesota Supercomputing Institute. The costs of publication of this article were defrayed in part by the payment of page charges. This article must therefore be hereby marked "*advertisement*" in accordance with 18 U.S.C. Section 1734 solely to indicate this fact.

[1] Supported by a postdoctoral fellowship from the government of the Republic of Vietnam. Present address: Inst. of Biotechnology, Vietnamese Academy of Science & Technology, Hanoi, Vietnam.

[2] Present address: College of Pharmacy, Medical University of South Carolina, Charleston, SC 29425.

[3] Both authors contributed equally to this work.

[4] To whom correspondence should be addressed: Div. of Oncology Research, Guggenheim 1342C, Mayo Clinic, 200 First St. S. W., Rochester, MN 55905. Tel.: 507-284-8950; Fax: 507-284-3906; E-mail: Kaufmann.scott@mayo.edu.

[5] The abbreviations used are: ROS, reactive oxygen species; CM-H_2DCF, 5(6)-chloromethyldihydro-2′,7′-dichlorofluorescein; CysNAc, *N*-acetylcysteine; CM-DCF, 5(6)-chloromethyl-2′,7′-dichlorofluorescein; CCCP, carbonyl cyanide 3-chlorophenylhydrazone; BSO, buthionine sulfoximine; TPP^+, tetraphenylphosphonium cation; DPBS, calcium- and magnesium-free Dulbecco's phosphate-buffered saline; HPLC, high performance liquid chromatography; LC-MS/MS, liquid chromatography-tandem mass spectrometry; MOPS, 3-(*N*-morpholino)propanesulfonic acid; MIB, mitochondrial incubation buffer.

drug-sensitive transporters (7, 8), raising some doubt regarding the role of ROS in adaphostin cytotoxicity.

In biological systems, quinones are known to undergo enzymatic reduction to semiquinone radicals, which then spontaneously oxidize back to quinones, generating superoxide anion in the process (9–12). These prior observations have led to a general assumption that adaphostin might be rapidly oxidized either extracellularly or intracellularly to a quinone derivative, which could then generate ROS through redox cycling. Direct observations testing this hypothesis have not been reported, however. Moreover, the possibility that leakage of electrons from the mitochondrial electron transport chain, another common source of ROS (13–15), might contribute to the efficacy of adaphostin has not been examined previously.

In this study, we confirmed that adaphostin induces oxidative damage of DNA in intact cells and then followed the fate of adaphostin in solution and in intact cells. The results of this analysis demonstrate that adaphostin is concentrated several thousandfold in mitochondria, where it inhibits complex III of the respiratory chain and leads to mitochondrial ROS generation. These observations not only provide new insight into the mechanism of action of a promising anti-leukemic agent, but also provide additional support for the view that certain inhibitors of mitochondrial respiration might be potential anticancer agents.

MATERIALS AND METHODS

Reagents—Adaphostin (NSC680410) and its quinone derivative were synthesized by the Drug Synthesis and Chemistry Branch, Division of Cancer Treatment and Diagnosis, NCI, National Institutes of Health (Bethesda, MD). Reagents were purchased from the following suppliers: H_2O_2, tetrapropylammonium hydroxide, rotenone, carbonyl cyanide 3-chlorophenylhydrazone (CCCP), pyruvate, sodium succinate, CysNAc, ascorbic acid, butylated hydroxyanisole, *p*-iodonitrotetrazolium violet, phenazine methosulfate, decylubiquinone, bovine heart cytochrome *c*, carnitine, NAD^+, thiamine pyrophosphate, CoA, bongkrekic acid, *N*,*N*,*N*′,N′-tetramethyl-*p*-phenylenediamine, bovine erythrocyte superoxide dismutase, uridine, and catalase from Sigma; buthionine sulfoximine (BSO) from Chemical Dynamics, Inc. (South Plainfield, NJ); CM-H_2DCF diacetate, dihydroethidium, and the Amplex Red H_2O_2 kit (catalog no. A-22188) from Molecular Probes (Eugene, OR); *N*-(*N*$^{\alpha}$-benzyloxycarbonyl-Val-Ala)-Asp(*O*-methyl ester)-fluoromethyl ketone from BIOMOL (Plymouth Meeting, PA); and formamidopyrimidine-DNA glycosylase from New England Biolabs (Ipswich, MA). All components for manufacturing a tetraphenylphosphonium cation (TPP^+)-selective membrane, including polyvinyl chloride, TPP sodium salt, and tetrahydrofuran, were from Fluka (Buchs, Switzerland). 2-[^{14}C]Thymidine (59 mCi/mmol) was from ICN (Irvine, CA).

Tissue Culture—K562 human leukemia cells and A549 non-small cell lung cancer cells (American Type Culture Collection, Manassas, VA) were grown in RPMI 1640 medium containing 5% (v/v) heat-inactivated fetal bovine serum, 100 units/ml penicillin G, 100 μg/ml streptomycin, and 2 mM glutamine. HCT116 human colon cancer cells and OVCAR5 human ovarian cancer cells were propagated in RPMI 1640 medium containing 10% (v/v) heat-inactivated fetal bovine serum, 100 units/ml penicillin G, 100 μg/ml streptomycin, and 2 mM glutamine. The MOLT-4 human acute lymphocytic leukemia cell line and its rho^0 derivative, which was generated as described previously (16), were grown in the same medium supplemented with 50 μg/ml uridine and 100 μg/ml sodium pyruvate.

To assess cell volume, photos of cells were taken using a Zeiss Axiovert 200M optical morphology microscope. The images were captured with a Zeiss Axiocam high resolution digital camera controlled with Zeiss KS400 software, which was used to measure the diameters of at least 80–100 individual cells from each line. The volumes of the cells were derived from the mean diameters and used in calculations to determine adaphostin whole cell uptake.

Colony-forming assays, which were performed as described previously (17, 18), were utilized to determine the effects of adaphostin on long-term viability of adherent cell lines. In brief, aliquots containing 350–500 cells were plated in replicate 35- or 60-mm tissue culture plates and allowed to adhere overnight. Cells were then treated with the indicated concentrations of BSO or CysNAc for 4 h, at which time adaphostin was added (without removal of BSO or CysNAc) for 24 h. At completion of the incubation, cells were washed, incubated for 7–8 days, stained with Coomassie Blue, and manually examined for colony formation. Diluent-treated plates typically contained 150–250 colonies.

Assessment of Intracellular ROS—CM-H_2DCF diacetate (a cell-permeant non-fluorescent compound that diffuses into cells, undergoes de-esterification, and is oxidized to the fluorescent dye CM-DCF) was used to assess changes in relative intracellular ROS levels. After exposure to drugs for the indicated times, cells were collected by centrifugation, incubated with 10 μM CM-H_2DCF diacetate in calcium- and magnesium-free Dulbecco's phosphate-buffered saline (DPBS) for 30 min in the dark at 37 °C, washed with DPBS, read on the FL1 channel of a BD Biosciences FACSCalibur, and analyzed using BD Biosciences CellQuest software.

Measurement of Adaphostin-mediated Superoxide and Peroxide Generation in Vitro—Superoxide radical generation was assessed using a cytochrome *c* reduction assay (19). Briefly, the reaction was initiated by the addition of adaphostin or diluent to a 1-ml mixture containing 50 μM oxidized cytochrome *c* and 50 mM Tris-HCl (pH 8.0) in the absence or presence of 30 μg/ml bovine erythrocyte superoxide dismutase. The level of superoxide generation was estimated from the difference in absorbance at 550 and 418 nm, which was measured after 1 h of incubation at 21 °C. Generation of H_2O_2 in solution was assessed using an Amplex Red assay, which monitors peroxidase-catalyzed oxidation of Amplex Red to resorufin (20), as described by the supplier. Known concentrations of H_2O_2 provided a standard curve.

Alkaline Elution with Formamidopyrimidine-DNA Glycosylase (Adapted from Refs. 21 and 22)—Logarithmically growing cells were labeled for 24 h with 1 μM [^{14}C]thymidine, sedimented, and incubated for 1–2 h at 37 °C in fresh culture medium. After incubation for 30 min at 37 °C with the indicated concentrations of adaphostin, H_2O_2, or vehicle, cells (~200,000/aliquot)

were deposited on Nucleopore phosphocellulose filters (1-μm pore size; VWR Scientific Products, Minneapolis, MN) by gentle suction. Cells were washed with 20 ml of ice-cold pre-lysis buffer (0.075 M NaCl and 0.024 M Na_4EDTA (pH 7.4)) and lysed by allowing 5 ml of buffer A (2% (w/v) SDS, 100 mM glycine, and 25 mM EDTA (pH 10)) to drip through the filters over 30 min. After the filters were washed with 25 ml of buffer B (40 mM HEPES-KOH (pH 8.0), 0.1 M KCl, 0.5 mM EDTA, and 0.2 mg/ml bovine serum albumin), 2 ml of buffer B containing 8 units/ml formamidopyrimidine-DNA glycosylase was added to each filter, which was then incubated at 37 °C for 30 min and washed with an additional 25 ml of buffer B. Prior to elution, 5 ml of buffer A with 0.5 mg/ml proteinase K was allowed to drip through the filter over 30 min. Filters were then washed with 20 mM EDTA (pH 10), and DNA was eluted with 20 mM EDTA (adjusted to pH 12.1 with tetrapropylammonium hydroxide). The distribution of radiolabel in the eluate, the tubing of the elution apparatus, and the filter was analyzed as described by Covey *et al.* (23). Cells that received 150–900 centigrays of γ-irradiation from a ^{137}Cs source were included in each experiment to provide a standard curve.

Analysis of Adaphostin Degradation in DPBS—Adaphostin was added to DPBS and incubated as indicated below. Aliquots were injected onto a Beckman System Gold HPLC system and separated on a Beckman Ultrasphere ODS 5-μm column (4 mm × 25 cm) by isocratic elution with a mobile phase consisting of 1:1 acetonitrile and 2.5 mM ammonium formate (pH 4). Elution was monitored by absorbance at 305 nm.

Liquid Chromatography-Tandem Mass Spectrometry (LC-MS/MS) Analysis—The LC/MS system consisted of a Shimadzu HPLC system containing two LC-10ADvp pumps and an SIL-10ADvp autoinjector (injection volume of 60 μl) coupled to a Quattro micro triple quadrupole mass spectrometer (Waters Corp., Milford, MA). Separation was performed using a Brownlee NewGuard RP-18 7-μm pre-column (15 × 3.2 mm; Chrom Tech, Apple Valley, MN) and a Genesis Lightning C_{18} 120A 4-μm analytical column (10 cm × 2.1 mm; Jones Chromatography, Lakewood, CO). The mobile phase (flow rate of 0.20 ml/min) consisted of acetonitrile and 0.625 mM formate buffer (pH 4), initially at a 40:60 (v/v) ratio for 40 min and then ramped to 60% acetonitrile and held for 10 min.

Ionizations of adaphostin and the quinone of adaphostin were accomplished using an electrospray ionization probe operating in positive mode. Detection was accomplished by MS/MS using a daughter ion spectrum scan (m/z 45–450), looking for daughters of the specific parent ions at m/z 394 and 392 for adaphostin and the quinone, respectively. The scan time, cone voltage, and collision energy values were, 1.0 s, 30 V, and 15 eV, respectively. The source temperature, desolvation temperature, cone gas flow, and desolvation gas flow were 100 °C, 120 °C, 100 liters/h, and 250 liters/h, respectively. LC-MS/MS data were collected from 5 to 55 min after sample injection. Spectra and chromatograms were processed using Micromass MassLynx Version 3.5 software.

Cell Fractionation and Isolation of Mitochondria from K562 Cells (Adapted from Ref. 24)—All steps were performed at 4 °C. K562 cells (~10^8) were harvested by centrifugation at 100 × g for 5 min, washed twice with ice-cold DPBS, and resuspended in 5 ml of buffer C (20 mM HEPES-KOH (pH 7.5), 10 mM KCl, 3 mM $MgSO_4$, 1 mM EDTA, 1 mM EGTA, 1 mM dithiothreitol, 0.1 mM α-phenylmethylsulfonyl fluoride, and 250 mM sucrose). After 20 min on ice, cells were homogenized in a tight-fitting Dounce homogenizer until lysed (50 strokes). After the homogenate was sedimented at 800 × g, the pellet containing unbroken cells and nuclei was discarded, and the supernatant was sedimented at 10,000 × g for 15 min at 4 °C to obtain the mitochondrial fraction, which was resuspended in 5 ml of ice-cold buffer C and placed on ice for 15–30 min until used. The post-mitochondrial supernatant was sedimented at 100,000 × g for 1 h to separate the microsomal fraction (pellet) from the cytosol (supernatant). Alternatively, rat liver mitochondria were isolated by differential centrifugation as described (25, 26).

Measurement of Adaphostin Content in Cellular Fractions—After 6 volumes of acetonitrile was added to 1 volume of each subcellular fraction, samples were mixed thoroughly and centrifuged at 14,000 × g for 5 min. The supernatant was subjected to HPLC as described above with known concentrations of adaphostin as a standard. The pellet was hydrolyzed in 0.5 M NaOH and assayed for protein.

Measurement of $\Delta\Psi_m$ of Isolated Mitochondria Using a TPP^+-selective Electrode—The membrane potential and respiration of isolated mitochondria were recorded using a prototype multichannel recorder (ABMT-USA, Inc., Durham, NC). $\Delta\Psi_m$ was measured in incubation medium containing 200 mM mannitol, 75 mM sucrose, 5 mM KH_2PO_4, 5 mM pyruvate, 5 mM malate, 2 mM $MgCl_2$, 1 mM EGTA, and 10 mM MOPS (pH 7.35) using a home-made TPP^+-sensitive mini-electrode as described (27). Briefly, mitochondria (1 mg/ml protein) were added to the incubation medium containing 500 μM TPP chloride. $\Delta\Psi$ was calculated from the TPP^+ electrode reading according to the following equation: $\Delta\Psi = 59\log(\nu/V) - 59\log(10^{(E-E_0)/59} - 1)$, where $\Delta\Psi$ is the mitochondrial membrane potential (in millivolts); ν is the mitochondrial matrix volume (1.6 μl/mg of mitochondrial protein) (28); V is the volume of the incubation medium (1 ml); and E_0 and E are electrode potentials (in millivolts) before and after the addition of mitochondria, respectively (29). Adaphostin up to 25 μM and vehicle (Me_2SO) up to 0.5% (v/v) did not interfere with the readings of the TPP^+-sensitive electrode. Only electrodes that exhibited a Nernstian response were used.

Oxygen Consumption—Mitochondria were suspended at a concentration of 1 mg/ml protein in mitochondrial incubation buffer (MIB) consisting of 200 mM mannitol, 75 mM sucrose, 5 mM KH_2PO_4, 2 mM $MgCl_2$, 1 mM EGTA, and 10 mM MOPS-KOH (pH 7.35). K562 cells were suspended in cell culture medium at a concentration of 10^7 cells/ml. Oxygen consumption was measured using a Clark-type electrode (Model 5300, YSI Inc.). All measurements were performed at room temperature.

Dehydrogenase Assays—Succinate dehydrogenase activity was assayed as described (30). Briefly, mitochondria (1 mg of protein) were suspended in 1 ml of reaction buffer containing 50 mM potassium phosphate (pH 7.4), 50 mM sodium succinate, 25 mM sucrose, 2 mM EDTA, and 0.1% (w/v) p-iodonitrotetrazolium violet and incubated on ice for 30 min. Following the addition of adaphostin, the suspension was incubated at 37 °C

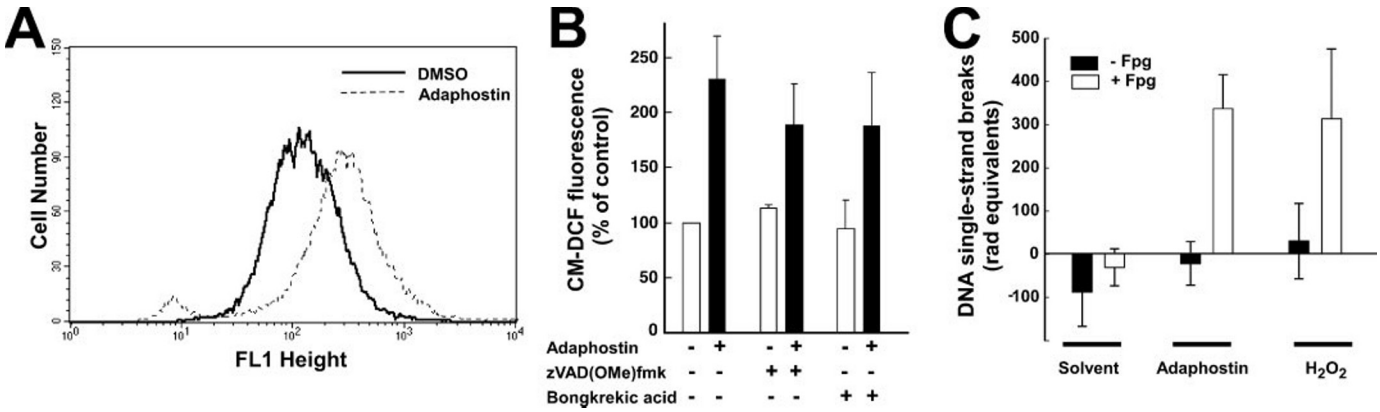

FIGURE 1. **Adaphostin induces ROS production and oxidative DNA damage.** *A*, K562 cells treated with adaphostin or diluent for 30 min were stained with CM-H_2DCF diacetate and subjected to flow cytometry. *B*, K562 cells were treated with diluent or 10 μM adaphostin in the absence or presence of 50 μM *N*-(*N*$^{\alpha}$-benzyloxycarbonyl-Val-Ala)-Asp(*O*-methyl ester)-fluoromethyl ketone (*zVAD(OMe)fmk*) or 50 μM bongkrekic acid for 30 min. Relative intracellular ROS levels were assessed using CM-H_2DCF diacetate. *C*, after K562 cells were treated with diluent, 10 μM adaphostin, or 10 μM H_2O_2 for 30 min, the presence of 8-oxoguanine was assessed by alkaline elution with or without formamidopyrimidine-DNA glycosylase (Fpg). Elution of DNA through the filters was compared with elution after irradiation of K562 cells with 400–800 centigrays of ionizing radiation. *Error bars* represent the means ± S.D. of three to five independent determinations.

for 15 min. After the reaction was terminated with 1 ml of 10% (w/v) trichloroacetic acid, the product was extracted into 4 ml of ethyl acetate and assayed at 490 nm.

Pyruvate dehydrogenase activity was measured as described by Schwab *et al.* (31). Briefly, mitochondria (4 mg/ml protein) were suspended in buffer consisting of 0.1% (v/v) Triton X-100, 1 mM $CaCl_2$, 5 mM $MgCl_2$, 50 mM KCl, 250 mM sucrose, and 20 mM Tris-HCl (pH 7.5). After three freeze-thaw cycles, mitochondria were incubated at 37 °C for 10 min to activate pyruvate dehydrogenase. Aliquots of the mitochondrial suspension (50 μl) were added to the wells of a microtiter plate, and the reaction was started by the addition of 250 μl of reaction buffer containing 5 mM L-carnitine, 2.5 mM NAD^+, 0.2 mM thiamine pyrophosphate, 0.1 mM CoA, 5 mM pyruvate, 0.1% (v/v) Triton X-100, 1 mM $MgCl_2$, 0.1% bovine serum albumin, 0.6 mM *p*-iodonitrotetrazolium violet, and 6.5 μM phenazine methosulfate in 0.05 M potassium phosphate (pH 7.5). Activity was estimated from the changes in absorbance ($A_{500} - A_{700}$).

Complex III Activity Measurement—Complex III activity was assessed by monitoring the reduction in cytochrome *c* measured as changes in absorbance ($A_{550} - A_{540}$) in the presence of reduced decylubiquinone (32). To synthesize reduced decylubiquinone, a small crystal of sodium borohydride was added to 200 μl of 10 mM decylubiquinone (oxidized form). 5 μl of 0.1 M HCl was added, and the reaction was mixed until the yellow solution became colorless. The reduced decylubiquinone (supernatant) was transferred to a fresh tube, diluted with 5 ml of 1 M HCl, and stored in the dark until used. To assay complex III activity, mitochondria (30 μg/ml protein) were resuspended in reaction buffer containing 250 mM sucrose, 1 mM EDTA, 50 mM Tris-HCl (pH 7.4), 50 μM cytochrome *c*, and 2 mM KCN at 21 °C. The reaction was initiated by the addition of 50 μM reduced decylubiquinone, and complex III activity was measured by monitoring changes in absorbance ($A_{550} - A_{540}$) over 3 min.

ROS Generation by Isolated Mitochondria—Rat liver mitochondria (1 mg/ml protein) in MIB supplemented with 5 mM succinate were snap-frozen in liquid nitrogen and thawed three times at 30 °C. After he addition of adaphostin and/or catalase, samples were incubated for 1 h at 30 °C. The concentration of H_2O_2 generated was assayed using Amplex Red (20) as described above.

Docking of Adaphostin into the Drug-binding Sites of the Cytochrome bc_1 Complex in Silico—Four different conformations of adaphostin were docked into two binding sites of the heme b_H-containing cytochrome *b* subunit of the cytochrome bc_1 complex using the EUDOC program with rotational and translational increments of 10° of arc and 0.5 Å, respectively (33). The atomic charges of adaphostin were generated according to the RESP procedure (34) with *ab initio* calculations at the HF/6-31G* level using the Gaussian 03 program (35). The adaphostin conformations were generated by systematically altering the conformation-governing torsions and subsequently optimized by energy minimizations using the force field (parm99.dat) of Cornell *et al.* (36) and the SANDER module of AMBER5 (37). The energy minimizations were monitored for reaching local minimum conformations with a normal mode analysis using the NMODE module of AMBER8 (37) and then terminated when the analysis showed that adaphostin reached a local minimum potential energy conformation. The first binding site of the holocytochrome *b* subunit, reported as the quinone reduction (Q_i) site (38), was taken from a crystal structure of the subunit containing antimycin A in the Q_i site (Protein Data Bank code 1NTK). The docking box (6.0 × 6.0 × 6.0 Å^3) at the Q_i site was defined to be surrounded by Phe^{18}, Ser^{35}, Leu^{197}, and heme b_H. The second binding site of the holosubunit, reported as the quinol oxidation (Q_o) site (39), was obtained from a crystal structure of the subunit containing azoxystrobin in the Q_o site (Protein Data Bank code 1SQB). The docking box (6.0 × 6.0 × 6.0 Å^3) at the Q_o site was defined to be surrounded by Phe^{128}, Tyr^{131}, Ile^{146}, Pro^{270}, and Phe^{274}. The EUDOC-generated adaphostin complex with the lowest interaction energy was then refined with 20 different molecular dynamics simulations (1.0 ns for each simulation with a 1.0-fs time step and different initial velocities) according to a published procedure (40) using the PMEMD module of AMBER8.

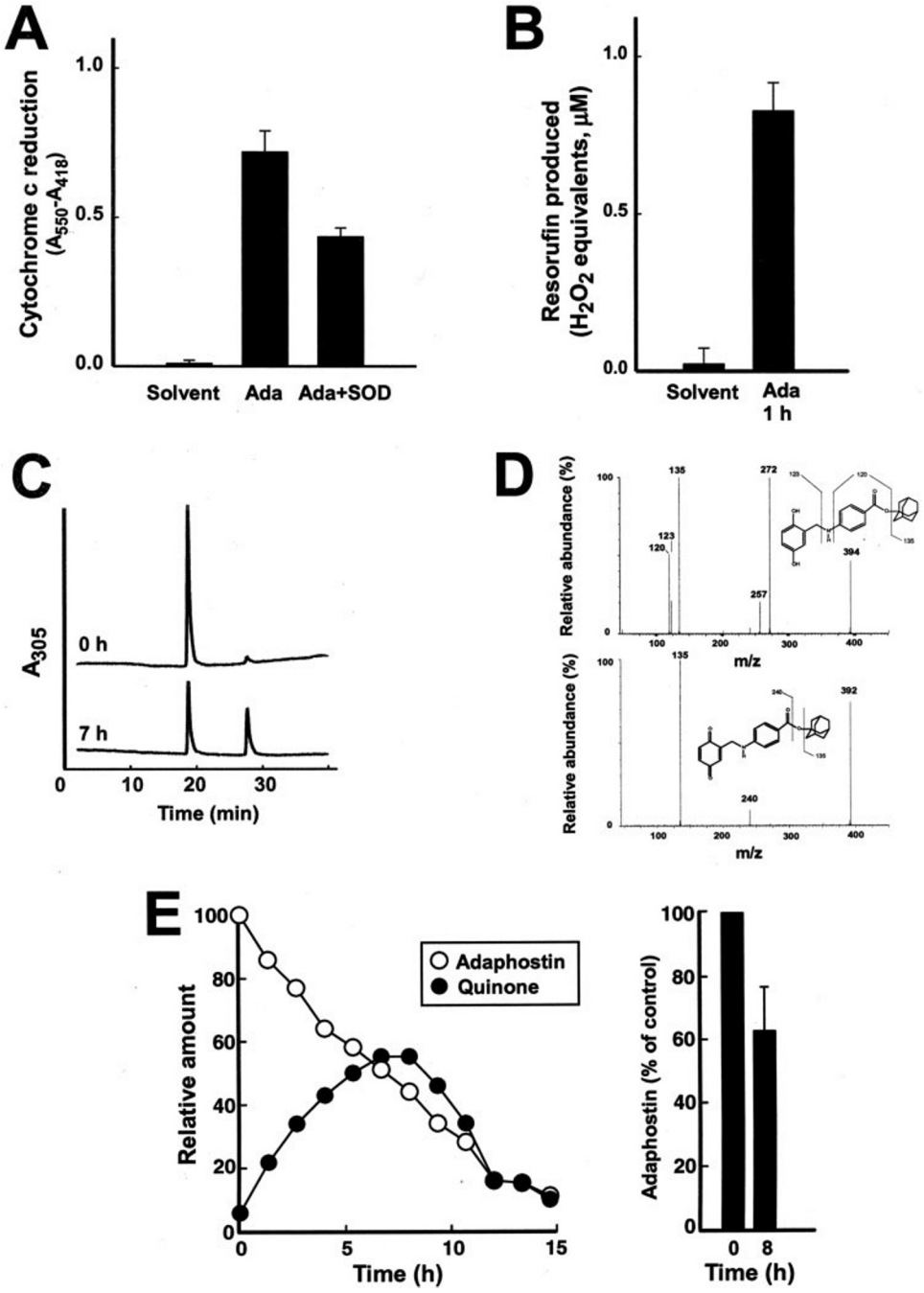

FIGURE 2. **Adaphostin generates ROS in DPBS and undergoes chemical transformation.** *A*, adaphostin (*Ada*; 100 μM) was added to buffer consisting of 50 μM cytochrome *c* in 50 mM Tris-HCl (pH 8) in the absence or presence of 30 μg/ml superoxide dismutase (*SOD*). After incubation for 1 h, the level of reduced cytochrome *c* was measured as the absorbance difference at 550 and 418 nm. *B*, shown is the H_2O_2 generation by 100 μM adaphostin during a 1-h incubation in DPBS. Amplex Red oxidation was assessed spectrophotometrically and compared with results obtained with known amounts of H_2O_2. *C*, adaphostin was added to DPBS and incubated for 7 h at room temperature. Aliquots were removed and subjected to HPLC. *D*, shown are the results from LC-MS/MS analysis of adaphostin (*upper panel*) and the product shown in *C* (*lower panel*). Positive electrospray ionization was used to generate the precursor ions $MH^+ = 394$ (*upper panel*) and $MH^+ = 392$ (*lower panel*), which were then subjected to collision-induced dissociation to produce the daughter ions shown in these product spectra. The adaphostin structure (*upper panel*), the deduced structure of the product (*lower panel*), and the collision-induced dissociation fragmentation resulting in the observed product ions are shown in the *insets*. The retention time and daughter ion spectrum of the product were identical to those of the *bona fide* quinone of adaphostin. *E*, adaphostin was added to DPBS and incubated at room temperature. Aliquots removed at the indicated time points were subjected to HPLC to assess adaphostin and quinone concentrations. *Left panel*, results showing the parent adaphostin and quinone measured simultaneously; *right panel*, pooled results of four experiments. *Error bars* represent the means ± S.D. of three (*A* and *B*) and four (*E*) independent determinations.

An average of 10,000 trajectories obtained at 1.0-ps intervals during the last 0.5-ns period of the 20 simulations was used as the refined three-dimensional model of the adaphostin complex.

Statistical Analysis—Values provided below represent the means ± S.D. of at least three independent experiments. *Error bars* in individual figures represent the means ± S.D. of the number of independent experiments indicated in the corresponding figure legends.

RESULTS

Adaphostin Increases the Levels of ROS within Cells—Previous studies suggested that adaphostin causes an increase in intracellular ROS levels (4, 6). Consistent with these results, treatment of K562 human leukemia cells with 10 μM adaphostin for 30 min caused an increase in CM-DCF fluorescence to 230 ± 40% of control values (mean ± S.D., $n = 5$) (Fig. 1, *A* and *B*). This increase in ROS was not significantly altered when cells were treated with adaphostin in the presence of the mitochondrial permeability transition inhibitor bongkrekic acid or the broad-spectrum caspase inhibitor *N*-(N^{α}-benzyloxycarbonyl-Val-Ala)-Asp(*O*-methyl ester)-fluoromethyl ketone (Fig. 1*B*), placing the ROS generation upstream of mitochondrial permeability transition and caspase activation.

Because alternative explanations, including adaphostin-induced inhibition of CM-DCF transporters (7, 8), might account for the increased CM-DCF fluorescence, additional experiments using alternative methods were performed to verify that adaphostin induced an increase in intracellular ROS levels. In particular, after cells were treated with vehicle or adaphostin, DNA was subjected to filter elution in the absence or presence of formamidopyrimidine-DNA glycosylase, an enzyme that recognizes and cleaves at 8-oxoguanine residues (41). As indicated in Fig. 1*C*, the increase in strand breaks detected in DNA from adaphostin-treated cells after formamidopyrimidine-DNA glyco-

sylase incubation was similar to that detected in DNA from cells treated with 10 μM H_2O_2, providing independent evidence of adaphostin-induced oxidative stress. Collectively, all of the results in Fig. 1 suggest that cells treated with adaphostin sustain oxidative damage.

Fate of Adaphostin in Aqueous Media—To identify the ROS causing this damage, we initially examined the fate of adaphostin in aqueous buffer. When adaphostin was incubated in DPBS, multiple assays indicated the presence of increased ROS levels. In preliminary experiments, the addition of adaphostin to DPBS containing 2-methyl-6-(4-methoxyphenyl)-3,7-dihydroimidazo[1,2-*a*]pyrazin-3-one resulted in increased luminescence indicative of increased ROS levels (data not shown). Likewise, the oxidation of dihydroethidium to the fluorescent compound ethidium was increased by adaphostin. Because these assays do not clearly distinguish between superoxide anion and peroxides, two ROS that could potentially be generated during adaphostin oxidation, we employed more selective assays in additional experiments. As shown in Fig. 2*A*, adaphostin induced a reduction in cytochrome *c*. The ability of purified superoxide dismutase to blunt this reduction suggests that adaphostin generates superoxide anion in solution. Likewise, adaphostin enhanced the peroxidase-mediated oxidation of Amplex Red to resorufin (Fig. 2*B*), suggesting that adaphostin also induces generation of H_2O_2.

To determine the basis for the generation of these ROS, the fate of adaphostin was followed by HPLC. During the course of incubation in DPBS at ambient oxygen tension, the parent compound disappeared, with a half-life of 8 $\pm$ 2 h (mean $\pm$ S.D., n = 4), and a new peak appeared (Fig. 2, *C* and *E*). Based on a 2-Da decrease in the size of the parent ion and the fragmentation observed during LC-MS/MS, the new peak was identified as the quinone derivative of adaphostin (Fig. 2*D*). Additional experiments indicated that chemically synthesized quinone had an indistinguishable retention time and collision-induced dissociation spectrum during LC-MS/MS (data not shown). Time course experiments indicated that the quinone concentration peaked at 6.2 $\pm$ 0.4 h (n = 3) and subsequently declined as this compound was oxidized even further (Fig. 2*E*). Collectively, these observations indicate that adaphostin in aqueous buffers is oxidized to the corresponding quinone with concomitant formation of superoxide and H_2O_2.

Fate of Adaphostin in Intact Cells—Armed with the information that adaphostin can be converted to the corresponding quinone, we next examined the fate of adaphostin in intact cells. For this analysis, K562 cells (10^6/ml) were treated with 2.5 μM adaphostin for periods of up to 4 h, extensively washed, and then extracted for HPLC analysis. In contrast with results obtained when adaphostin was incubated in DPBS (Fig. 2), the quinone could not be detected in the reducing environment of intact cells (Fig. 3*A*). Instead, only the parent drug was detected (Fig. 3*A*). Notably, however, this analysis also indicated that adaphostin was concentrated by 300 $\pm$ 30-fold (n = 3) in intact K562 cells relative to the extracellular medium (Fig. 3*B*). As a consequence, 38 $\pm$ 8% of the total drug added to the tissue culture medium was recovered with the cell pellet under the conditions of this incubation (Fig. 3*C*).

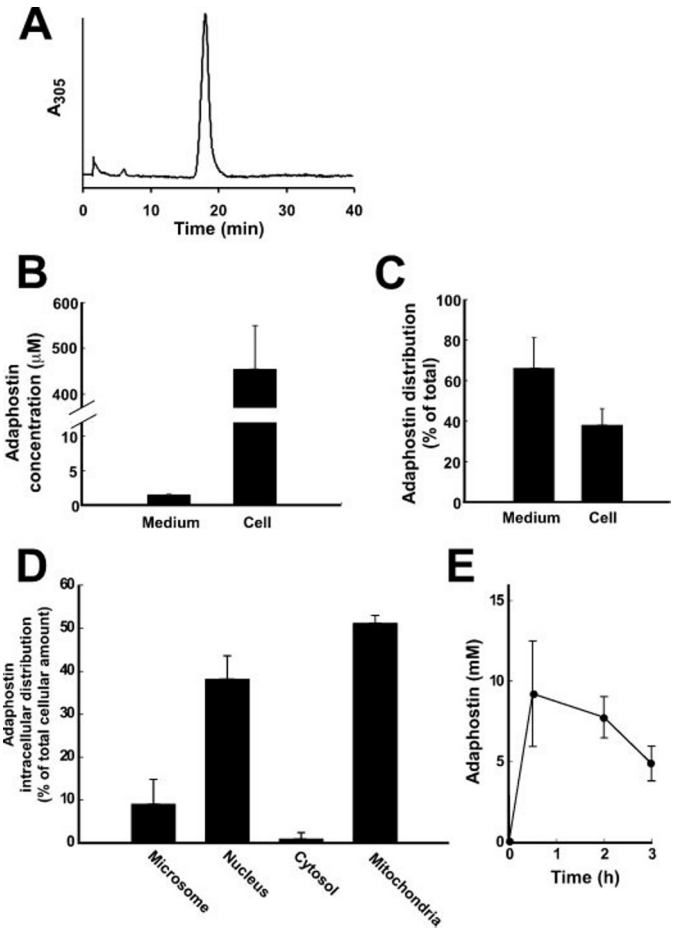

FIGURE 3. **Adaphostin uptake into K562 cells.** *A*, K562 cells were treated with 2.5 μM adaphostin for 30 min. Adaphostin uptake was analyzed by HPLC as described under "Materials and Methods." *B*, based on HPLC analysis, the concentration of adaphostin in the extracellular medium and cells was calculated. *C*, based on the experiment in *B*, the percentage of total adaphostin in the extracellular medium and cells is shown. *D*, after K562 cells were treated with 2.5 μM adaphostin for 30 min, subcellular fractions were isolated. Adaphostin content was measured in each fraction by HPLC. *E*, after K562 cells were treated with 2.5 μM adaphostin for different lengths of time, mitochondria were isolated. The amount of adaphostin in mitochondria was assessed by HPLC and is expressed in millimolar concentrations based on the assumption of a mitochondrial volume of 1.6 μl/mg of mitochondrial protein (28). *Error bars* represent the means $\pm$ S.D. of three independent determinations.

Using the approach described under "Materials and Methods," the subcellular distribution of adaphostin was examined by cell fractionation. As indicated in Fig. 3*D*, over half of all adaphostin taken into cells was recovered in the mitochondrial fraction. Assuming a mitochondrial volume of 1.6 μl/mg of mitochondrial protein (28), the final concentration of adaphostin in mitochondria was 9.2 $\pm$ 3.3 mM after treatment of the cells with 2.5 μM extracellular adaphostin, indicating an ~3000-fold concentration of drug in mitochondria. Time course experiments demonstrated that this dramatic uptake of adaphostin into mitochondria occurred in <30 min and persisted for at least 2–3 h (Fig. 3*E*). Further analysis demonstrated that similar mitochondrial concentrations could be achieved by incubating isolated mitochondria with 200 μM adaphostin under cell-free conditions, providing a means of reproducing the effects of adaphostin under cell-free conditions in the experiments described below.

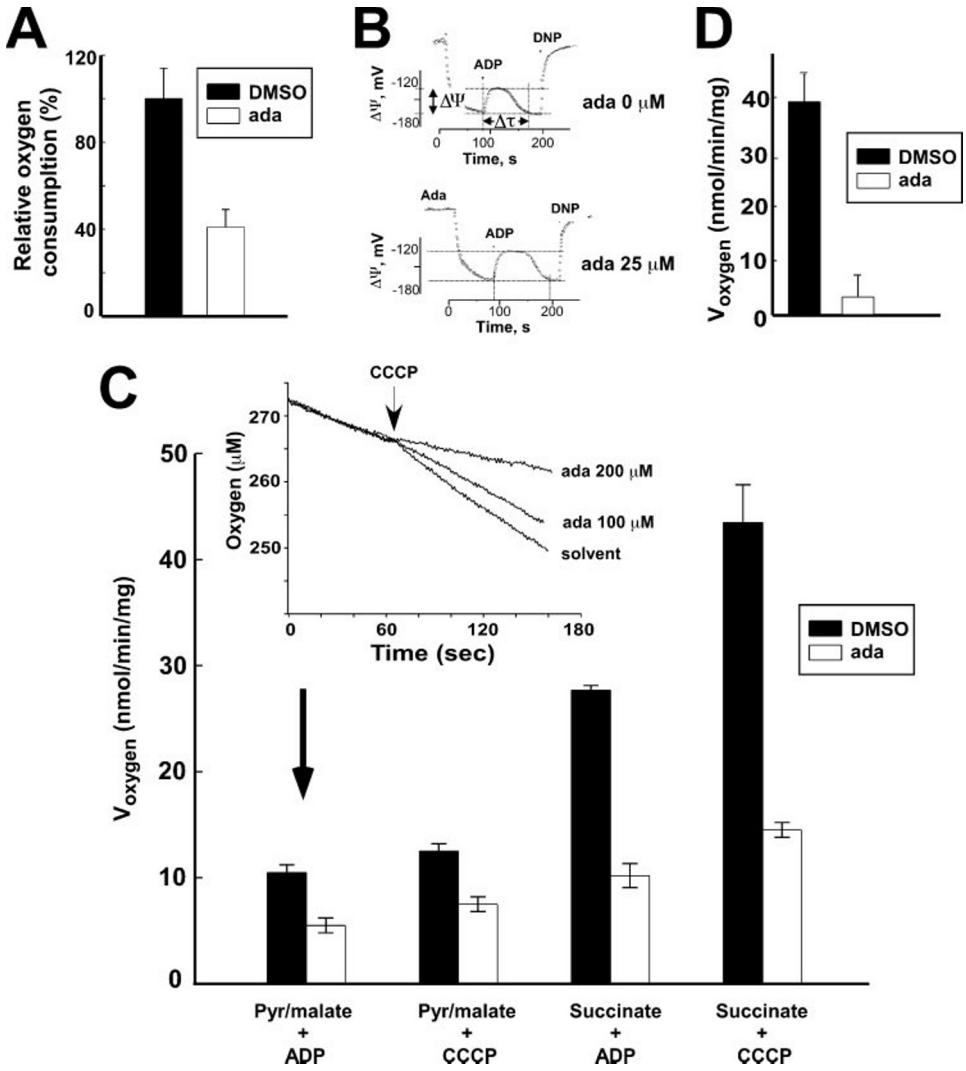

FIGURE 4. **Adaphostin inhibits mitochondrial respiration.** *A*, effect of adaphostin on oxygen consumption in intact K562 cells. K562 cells (10^7/ml) were added to a closed chamber with an oxygen electrode at room temperature. After the addition of diluent (dimethyl sulfoxide (*DMSO*)) or adaphostin (*ada*) and 1 μM CCCP, oxygen levels were monitored, and the rate of oxygen consumption was calculated. *B*, isolated rat liver mitochondria were added to a TPP^+-containing solution supplemented with diluent or 25 μM adaphostin in a cuvette with a TPP^+-sensitive electrode for measurement of mitochondrial transmembrane potential. At the indicated times, 300 μM ADP was added. DNP (2,4-dinitrophenol; 10 μM) was subsequently added to dissipate the transmembrane proton gradient. The time required for mitochondria to recover from depolarization ($\Delta\tau$) was delayed in the presence of 25 μM adaphostin. *C*, isolated rat liver mitochondria were added to buffer containing either 5 mM succinate and 1 μM rotenone or 5 mM pyruvate (*Pyr*) and 5 mM malate in the absence or presence of 100 μM adaphostin. The oxygen level was measured using a Clark-type electrode. After 1 min, 300 μM ADP or 0.4 μM CCCP was added. The rate of oxygen consumption by mitochondria was calculated after the addition of respiration stimuli (CCCP or ADP) and is expressed as nanomoles/min/mg of mitochondrial protein. *Inset*, plot of oxygen level *versus* time after the addition of CCCP in the presence of diluent or different adaphostin concentrations. Note that treatment of mitochondria with 200 μM adaphostin under cell-free conditions resulted in mitochondrial levels similar to those obtained by treating whole cells with 2.5 μM adaphostin. *D*, after isolated rat liver mitochondria were subjected to three cycles of freezing in liquid nitrogen, aliquots were added to MIB containing 1 mM NADH, and oxygen levels were measured using a Clark-type electrode. Adaphostin (200 μM) or diluent was added after 1 min. The rate of oxygen consumption by mitochondria after the addition of adaphostin or diluent was calculated. *Error bars* represent the means ± S.D. of three to five independent determinations.

Effect of Adaphostin on Mitochondrial Respiration—To assess whether adaphostin might alter mitochondrial function, we initially examined the effect of adaphostin on oxygen consumption in intact cells. In brief, the respiration of K562 cells was assessed using a closed chamber and a Clark-type oxygen sensor. The oxygen consumption of diluent- or adaphostin-treated cells was monitored in the absence and presence of CCCP, an uncoupler of mitochondrial oxidative phosphorylation. As indicated in Fig. 4*A*, adaphostin diminished the CCCP-uncoupled oxygen consumption rate in intact cells by 59 ± 8% ($n = 3$), raising the possibility that adaphostin might affect mitochondrial function.

To further analyze this possibility, we examined the effect of adaphostin on ADP-induced depolarization of isolated mitochondria using an ion-sensitive electrode (26, 27). These and subsequent experiments utilized mitochondria from rat liver because of the ability to isolate large quantities of highly purified organelles from this tissue. The addition of 300 μM ADP to these mitochondria resulted in transient depolarization during the period of ATP synthesis, followed by repolarization to a steady-state $\Delta\Psi_m$ of −170 mV (Fig. 4*B*, *upper panel*). Treatment with 25 μM adaphostin caused prolongation of the ADP-induced mitochondrial depolarization (Fig. 4*B*, *lower panel*), suggesting that adaphostin might inhibit some component of the mitochondrial respiratory chain, nucleotide exchange, or mitochondrial F_0F_1-ATPase.

To examine the action of adaphostin on mitochondria in greater detail, the rate of oxygen consumption by isolated mitochondria was examined in the presence of various respiratory substrates. As indicated in Fig. 4*C* (*inset*), when mitochondria were incubated with the complex I substrates pyruvate and malate, adaphostin diminished ADP-induced mitochondrial oxygen consumption in a dose-dependent manner. On average, 200 μM adaphostin, which resulted in the same mitochondrial drug concentration as observed in intact cells treated with 2.5 μM adaphostin, caused a 48 ± 2% ($n = 3$) decrease in ADP-stimulated respiration (Fig. 4*C*). When the complex II substrate succinate was substituted for pyruvate and malate, adaphostin likewise caused a 63.2 ± 2.5% ($n = 3$) decrease in ADP-stimulated respiration (Fig. 4*C*). Moreover, adaphostin also inhibited CCCP-stimulated oxygen consumption in the presence of the same substrates (Fig. 4*C*). Because CCCP uncouples electron transport and ATP synthesis, making oxy-

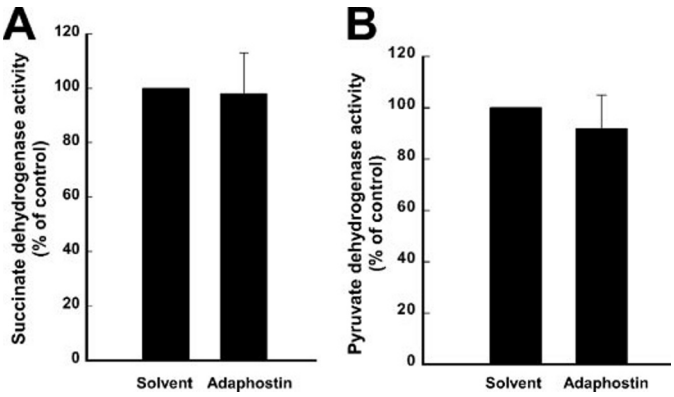

FIGURE 5. **Adaphostin fails to inhibit succinate or pyruvate dehydrogenase.** *A*, after 100 μM adaphostin or diluent was added to isolated rat liver mitochondria, succinate dehydrogenase (*A*) or pyruvate dehydrogenase (*B*) activity was measured as described under "Methods and Materials." *Error bars* represent the means ± S.D. of three independent determinations.

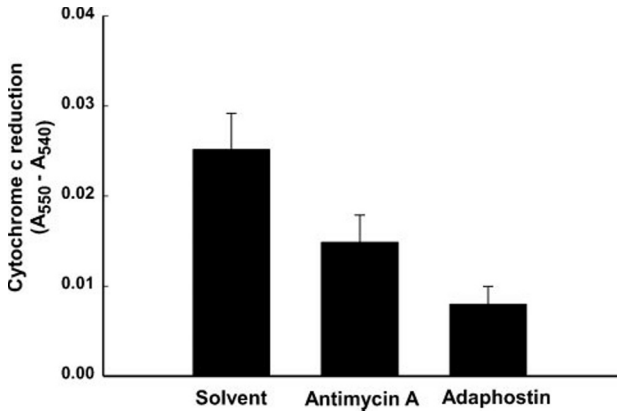

FIGURE 6. **Adaphostin inhibits complex III in the mitochondrial respiratory chain.** Rat liver mitochondria were assayed for site III activity as measured by reduced decylubiquinone-induced cytochrome *c* reduction in the presence or absence of 100 μM adaphostin. Antimycin (a known inhibitor of complex III activity) was used at 5 μg/ml as a positive control. *Error bars* represent the means ± S.D. of three independent determinations.

gen consumption independent of ATP generation, the observed ability of adaphostin to inhibit respiration of CCCP-treated mitochondria argued against the possibility that adaphostin inhibits the adenine nucleotide transporter or F_0F_1-ATPase.

A series of additional experiments were performed to further delineate the adaphostin-sensitive step in mitochondrial respiration. In these experiments, adaphostin failed to inhibit the succinate and pyruvate dehydrogenase complexes directly (Fig. 5, *A* and *B*), suggesting that the block is downstream of dehydrogenase activity. Moreover, when mitochondria were frozen and thawed repeatedly to disrupt the inner mitochondrial membrane, rendering it freely permeable to NADH (42, 43), adaphostin inhibited NADH-stimulated oxygen consumption (Fig. 4*D*), confirming that the effect of adaphostin is mediated by direct inhibition of mitochondrial electron transfer rather than inhibition of tricarboxylic acid cycle dehydrogenases. Additional experiments (not shown) failed to demonstrate any inhibition of oxygen consumption when isolated intact mitochondria were incubated with 1 mM ascorbic acid in the presence of *N*,*N*,*N*′,N′-tetramethyl-*p*-phenylenediamine, which transfers electrons to cytochrome *c* (44, 45), confirming that electron transfer from cytochrome *c* to cytochrome *c* oxidase to molecular oxygen was intact.

Collectively, the preceding experiments suggested that adaphostin might inhibit complex III. To test this hypothesis more directly, complex III activity was assessed by monitoring cytochrome *c* reduction in the presence of reduced decylubiquinone. Like the selective complex III inhibitor antimycin A (46), adaphostin inhibited decylubiquinone-induced cytochrome *c* reduction (Fig. 6).

Adaphostin Fits into the Q_i Site of Complex III—To gain further insight into the potential interaction of adaphostin with complex III, the docking of multiple conformations of adaphostin into two known binding sites of the heme b_H-containing cytochrome *b* subunit of the cytochrome bc_1 complex (38, 39) was analyzed *in silico*. This analysis suggested that adaphostin preferentially binds to the Q_i site (−28 kcal/mol for the Q_i site *versus* more than −5 kcal/mol for the Q_o site). In the refined three-dimensional model of the adaphostin complex with an intermolecular interaction energy of −47.3 kcal/mol (E_{vdW} = −45.6 kcal/mol and E_{ele} = −1.7 kcal/mol), the adamantyl group of adaphostin has van der Waals interactions with the methyl group of heme b_H and with the side chains of Gly^{38}, Leu^{41}, Ile^{42}, Met^{190}, and Met^{194}; the middle and terminal aromatic groups of the drug form π-π interactions with the side chains of Phe^{18} and Phe^{220}, respectively; the *meta*-hydroxyl group of the drug has a water-bridged hydrogen bond with Asn^{32} and Ser^{35}; and the *ortho*-hydroxyl group has a water-bridged hydrogen bond with Ser^{205} (Fig. 7*A*). Interestingly, the binding mode of adaphostin is very similar to that of antimycin A, as shown in Fig. 7 (*B* and *C*), even though the adaphostin model was computationally developed without any assumption that adaphostin shares the binding mode of antimycin A.

Generation of ROS by Adaphostin-treated Mitochondria—The preceding analysis suggested that inhibition of complex III is a primary effect of adaphostin. To rule out the alternative hypothesis that the effects of adaphostin on mitochondrial respiration are due to adaphostin-induced spontaneous generation of ROS in solution (Fig. 2), followed by ROS-induced inhibition of respiration (47), the effect of adaphostin on mitochondrial oxygen consumption was examined in the absence and presence of butylated hydroxyanisole or CysNAc, two antioxidants with different chemical structures. As indicated in Fig. 8*A*, neither of the antioxidants reversed the inhibitory effect of adaphostin on mitochondrial respiration. These results provide further evidence that inhibition of mitochondrial respiration is a primary effect of adaphostin rather than a consequence of ROS generation.

An additional series of experiments assessed whether the effects of adaphostin on mitochondrial function (Figs. 4–6) could contribute to the increased ROS levels observed in intact cells (Fig. 1). For these experiments, H_2O_2 production (13, 47) was assessed after mitochondria were incubated with diluent or adaphostin in the absence or presence of catalase. Consistent with our previous results (Fig. 2*B*), adaphostin by itself generated H_2O_2 in solution (Fig. 8*B*). In the presence of mitochondria, however, the amount of ROS generated increased at least 7-fold, suggesting that the effects of adaphostin on mitochon-

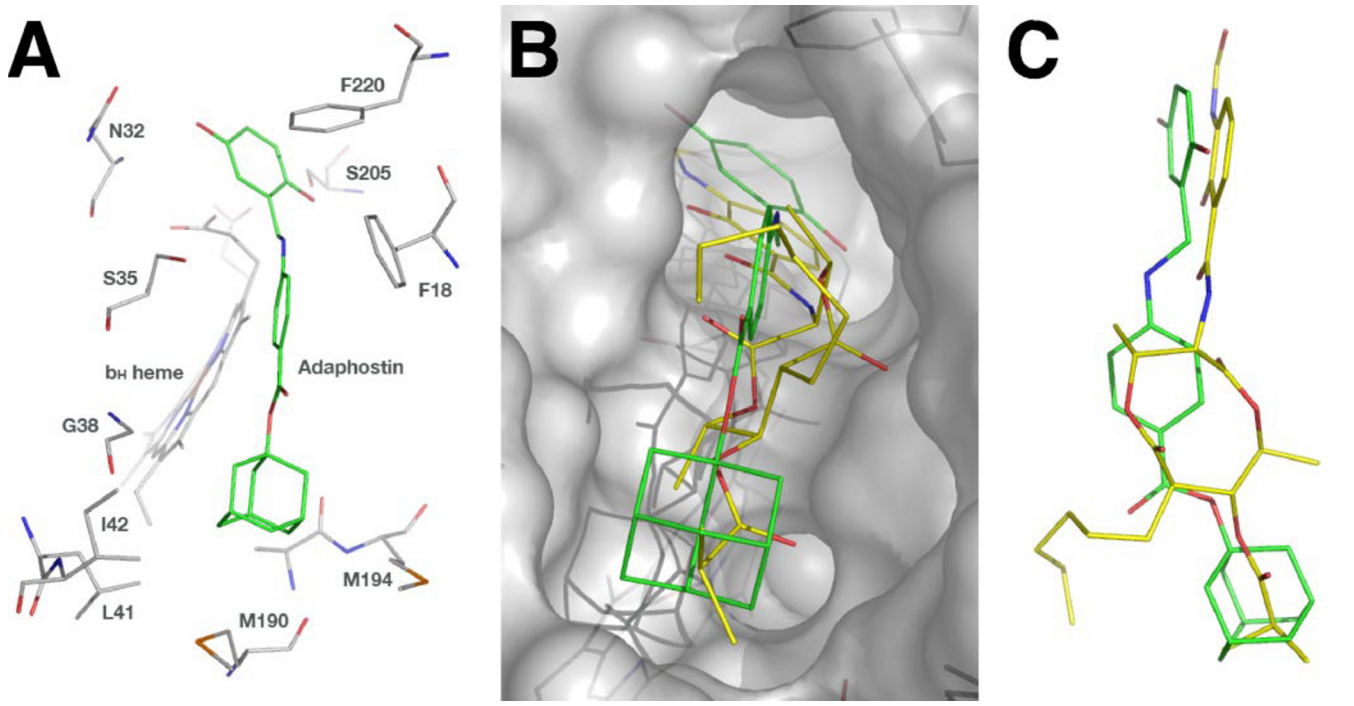

FIGURE 7. **Docking of adaphostin into the Q_i site of cytochrome *b in silico*.** *A*, close-up view of adaphostin bound in the Q_i site of the cytochrome *b* subunit of the cytochrome bc_1 complex; *B* and *C*, overlays of the adaphostin complex (*green*) with the antimycin A complex (*yellow*).

drial respiration contribute substantially to ROS generation by this agent.

To further examine the role of mitochondrial electron transport in adaphostin-induced ROS, the MOLT-4 human leukemia cell line and a rho^0 derivative that lacks mitochondrial electron transport as a consequence of loss of mitochondrial DNA (16) were compared. Consistent with results in other cell lines (Fig. 1) (4, 6), treatment of MOLT-4 cells with 10 μM adaphostin for 30 min caused an increase in CM-DCF fluorescence to 200 ± 11% of control values (mean ± S.D., $n = 4$) (Fig. 8, *C* and *D*). In contrast, treatment of MOLT-4 rho^0 cells with adaphostin resulted in more uptake into cells (Fig. 8*D*, *inset*), but caused only a 24 ± 14% increase in CM-DCF fluorescence (Fig. 8, *C* and *D*), suggesting that 75% of the adaphostin-induced increase in ROS levels in parental MOLT-4 cells depends on ongoing mitochondrial electron transport.

ROS-dependent Cytotoxicity in Solid Tumor Cell Lines—Because the ability to inhibit complex III and to increase ROS levels should not be limited to leukemia cell lines, we examined the effect of adaphostin in widely studied solid tumor cell lines. As indicated in Fig. 9*A*, treatment of HCT116 human colon adenocarcinoma cells with 10 μM adaphostin for 30 min caused an increase in CM-DCF fluorescence to 195 ± 7% of control values (mean ± S.D., $n = 4$). Additional experiments (not shown) indicated that adaphostin was concentrated 80-fold in these cells relative to the extracellular medium. To assess the impact of the increased ROS levels, cells were exposed for 24 h to adaphostin, washed, and assayed for the ability to subsequently proliferate into colonies. Treatment with adaphostin inhibited HCT116 colony formation in a dose-dependent manner (Fig. 9*C*), with $IC_{90} = 17 \pm 3$ μM (mean ± S.D., $n = 4$). CysNAc at 6 mM, one-fourth of the concentration used previously (4), diminished the anti-proliferative effects at the highest adaphostin concentration tested (Fig. 9*C*).[6] Conversely, glutathione depletion with BSO diminished the IC_{90} by 4.5 ± 1.9-fold (mean ± S.D., $n = 4$). In A549 non-small cell lung cancer cells, which took up 8-fold less adaphostin than HCT116 cells, the increase in ROS levels after exposure to 10 μM adaphostin was much lower (Fig. 9*B*), and the anti-proliferative effects of adaphostin were less potent (Fig. 9*D*), with $IC_{90} = 33 \pm 3$ μM ($n = 3$). Nonetheless, treatment with CysNAc at 24 mM protected the cells at multiple adaphostin concentrations, and BSO treatment again diminished the IC_{90} by a factor of 7.65 ± 1.2 ($n = 3$) (Fig. 9*D*). Similar results were observed in OVCAR5 ovarian cancer cells (data not shown). Collectively, these results indicate that adaphostin is concentrated in solid tumor cell lines, that it generates ROS, and that the ability of solid tumor cells to detoxify these ROS plays an important role in resistance to this agent.

DISCUSSION

Because adaphostin demonstrates activity against a wide range of hematological malignancies *in vitro*, there is considerable interest in understanding its mechanism of action. This study has demonstrated that adaphostin generates ROS within intact cells and causes oxidative DNA damage. Additional experiments designed to identify the source of these ROS indicated that adaphostin is oxidized to the corresponding quinone in aqueous buffers. In the reducing environment of the intact cell, however, the quinone is not detectable. Instead, adaphostin is concentrated by up to 3000-fold in mitochondria, where it inhibits respiratory complex III. Consistent with previous reports that inhibition of mitochondrial electron transport can

[6] Higher CysNAc concentrations could not be utilized because they diminished HCT116 cell colony formation by themselves.

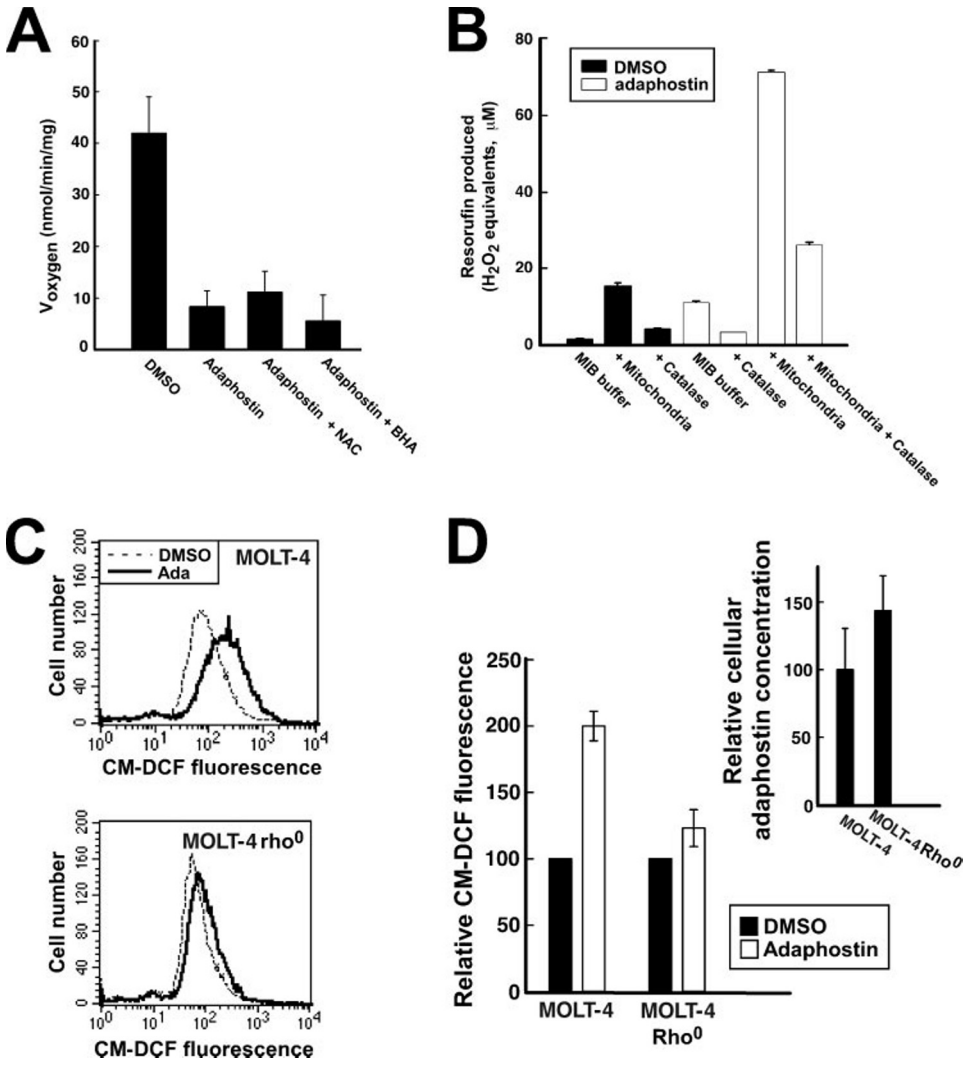

FIGURE 8. **Adaphostin-induced ROS generation in the presence of mitochondria.** *A*, adaphostin was added to isolated rat mitochondria in MIB containing 5 mM succinate, 1 μM rotenone, and 24 mM CysNAc (*NAC*) or 100 μM butylated hydroxyanisole (*BHA*). The CCCP-stimulated oxygen consumption rate was measured using an oxygen electrode as illustrated in Fig. 4. Extensive preliminary experiments indicated that CysNAc and butylated hydroxyanisole by themselves had no effect on rat mitochondrial oxygen consumption (data not shown). *B*, aliquots of MIB without or with isolated rat liver mitochondria (1 mg/ml protein) were incubated for 1 h at 37 °C in the absence or presence of 100 μM adaphostin and/or 600 units/ml catalase. At the completion of the incubation, Amplex Red was added to assay the H_2O_2 generated. *C*, MOLT-4 cells (*upper panel*) or MOLT-4 rho^0 cells (*lower panel*) treated with 10 μM adaphostin (*Ada*) or diluent (dimethyl sulfoxide (*DMSO*)) for 30 min were stained with CM-H_2DCF diacetate and subjected to flow cytometry. *D*, shown is a summary of CM-H_2DCF diacetate staining experiments examining rho^0 cells. *Inset*, the cellular concentration of adaphostin in MOLT-4 rho^0 cells, determined as described in the legend to Fig. 3 (*B* and *E*), was compared with that in MOLT-4 cells in the same experiments. *Error bars* represent the means ± S.D. of three (*A*, *B*, and *inset* in *D*) and four (*D*) independent experiments.

result in generation of ROS (48–50), our study has also demonstrated increased ROS levels upon incubation of adaphostin with mitochondria under cell-free conditions. These results have potentially important implications for the current understanding of the cytotoxic action of adaphostin.

The results of previous studies demonstrated that treatment of cells with adaphostin results in enhanced CM-DCF fluorescence (4, 6), providing presumptive evidence of ROS generation. Additional experiments indicated that the cytotoxicity of adaphostin is enhanced by glutathione depletion and diminished by treatment with CysNAc (4, 6). The results of the present analysis confirmed and extended these previous findings by providing direct evidence of oxidative DNA damage after adaphostin treatment (Fig. 1*C*). These results rule out the possibility that the enhanced CM-DCF fluorescence merely represents an effect of adaphostin on ATP-binding cassette proteins (7, 8).

While this work was in progress, Hose *et al.* (51) reported that adaphostin treatment results in an increase in cytosolic free iron as assessed by decreased fluorescence of the iron-sensitive dye Phen Green SK and that the iron chelator desferrioxamine diminishes adaphostin-induced cytotoxicity, prompting the authors to conclude that mitochondrial release of iron contributes to the ROS elevation and cytotoxicity of adaphostin. Our subsequent experiments showed, however, that the diminished dye fluorescence might be a result of adaphostin-mediated quenching (26), that increased cytosolic iron could not be detected by mass spectroscopy,[7] and that desferrioxamine failed to protect K562 cells from adaphostin-induced cytoxicity.[7,8] These observations, which might differ from the results of Hose *et al.* because of cell type-specific differences in the effects of adaphostin on iron sequestration, prompted us to search further for the source of adaphostin-induced ROS.

Several lines of evidence indicate that this increase in ROS levels is independent of any inhibitory effect of adaphostin on Bcr/Abl. First, increased ROS levels are evident in K562 cells within 15–30 min (Fig. 1) (4), whereas inhibition of Bcr/Abl-mediated phosphorylation is not evident for 4–6 h (2). Second, inhibition of Bcr/Abl and Abl by imatinib mesylate is accompanied by decreased ROS levels (52), whereas adaphostin causes an increase in ROS levels. Finally, adaphostin-induced increases in ROS levels are observed in a variety of Bcr/Abl-negative cells, including the Jurkat, ML-1, MOLT-4, A549, and HCT116 cell lines, as well as in chronic lymphocytic leukemia and acute myelogenous leukemia clinical samples (Figs. 8*C* and 9) (4–6).

On the basis of the dihydroquinone structure of adaphostin, we anticipated that this compound might undergo oxidation to

[7] S. B. Lee and S. H. Kaufmann, unpublished data.
[8] J. Chandra, personal communication.

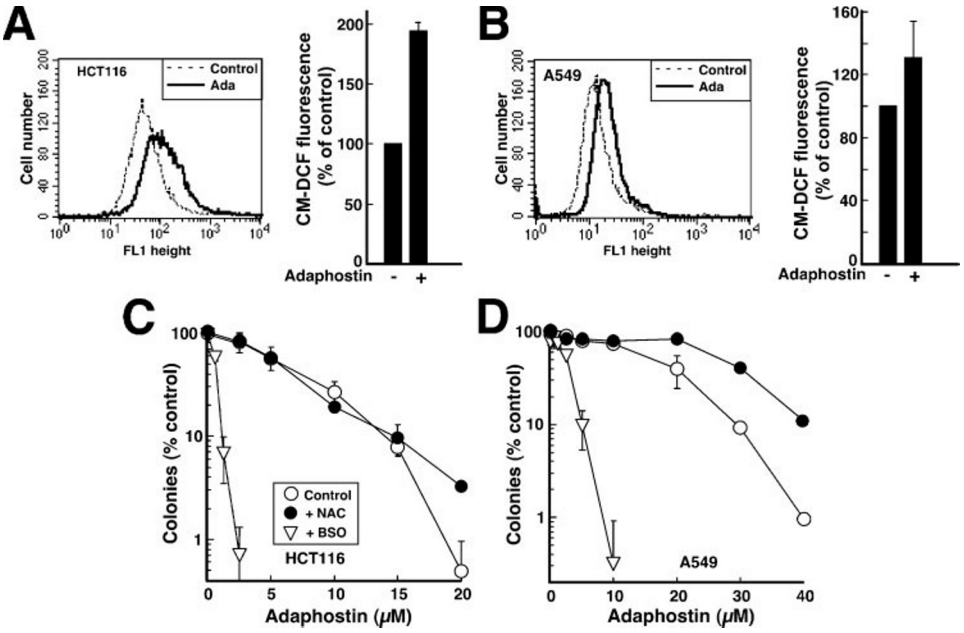

FIGURE 9. **Adaphostin-induced ROS generation and killing in solid tumor cell lines.** *A* and *B*: *left panels*, HCT116 and A549 cells, respectively, treated with 10 μM adaphostin (*Ada*) or diluent for 30 min were stained with CM-H_2DCF diacetate and subjected to flow cytometry. *Right panels*, the *bar graphs* indicate the means ± S.D. of three independent determinations. *C* and *D*, HCT116 and A549 cells, respectively, treated for 4 h with 6 mM (*C*) or 24 mM (*D*) CysNAc (*NAC*) or with 0.5 mM BSO were treated with the indicated concentrations of adaphostin for 24 h, washed, and allowed to form colonies. *Error bars* represent the means ± S.D. of triplicate determinations.

the corresponding quinone in aqueous buffer at ambient oxygen tension. Consistent with this hypothesis, the quinone derivative of adaphostin was readily detected, along with superoxide radical and H_2O_2, when adaphostin was incubated in aqueous buffers (Fig. 2, *A–D*). Under conditions encountered in cells, however, this oxidation was not detectable (Fig. 3*A*). Instead, adaphostin was concentrated 3000-fold in mitochondria (Fig. 3, *B–D*), where it inhibited mitochondrial respiration (Fig. 4) and contributed to generation of ROS (Fig. 8*B*).

It is important to emphasize that these effects of adaphostin on mitochondria are upstream rather than downstream of ROS generation. In particular, treatment of isolated mitochondria with adaphostin in the presence of ROS scavengers also inhibited mitochondrial respiration (Fig. 8*A*). These results suggest that adaphostin blocks mitochondrial respiration directly rather than by generating ROS, which in turn damage mitochondria and block electron transport. Moreover, adaphostin-induced increases in ROS levels were markedly diminished in cells lacking oxidative phosphorylation (Fig. 8, *C* and *D*), providing further support for the view that mitochondrial electron transport contributes to adaphostin-induced ROS.

Additional experiments demonstrated that adaphostin attenuated respiration of isolated mitochondria incubated with the complex I substrates pyruvate and malate (Fig. 4, *C* and *D*) or the complex II substrate succinate (Fig. 4*C*). Coupled with the failure of adaphostin to inhibit pyruvate and succinate dehydrogenases (Fig. 5), these results suggested that adaphostin might act downstream of complexes I and II. Consistent with this hypothesis, adaphostin was found to inhibit the ability of reduced decylubiquinone to reduce cytochrome *c* (Fig. 6). These results indicate that, like antimycin A and certain ubiquinone analogs (53–55), adaphostin is an inhibitor of respiratory complex III. Consistent with this possibility, an *in silico* docking study performed without any prior assumption about the mode of adaphostin binding to the Q_o and Q_i sites of cytochrome *b* demonstrated that the Q_i site could accommodate adaphostin in a binding mode similar to that of antimycin A (Fig. 7). Additional analysis demonstrated that, like antimycin A (48, 49), adaphostin enhanced mitochondrial generation of ROS (Fig. 8*B*), providing an explanation for the increased ROS in adaphostin-treated cells.

Despite the fact that adaphostin and antimycin A both inhibit complex III, there are important differences between these agents. A previous study suggested that antimycin A is a general cellular poison that exhibits little selectivity for neoplastic compared with normal cells (56). In contrast, previous studies have demonstrated that adaphostin is selective for chronic myelogenous leukemia (1, 2) and chronic lymphocytic leukemia (4, 5) compared with normal bone marrow progenitors and normal lymphocytes. Although the basis for this selectivity is currently unknown, previous studies have demonstrated enhanced uptake of a number of aromatic cationic dyes into the mitochondria of neoplastic cells (57–60). Additional experiments examining the mechanism of uptake of adaphostin into mitochondria are required to determine whether the propensity of mitochondria in neoplastic cells to concentrate aromatic cationic compounds contributes to the observed selectivity of adaphostin for leukemic as opposed to normal leukocytes.

Even though this study demonstrated a remarkable concentration of adaphostin within mitochondria, it is important to note that almost 40% of the total cellular drug was also found in nuclei. We cannot at present rule out the possibility that nuclear accumulation of adaphostin also contributes to the cytotoxicity of this agent. Nonetheless, previous results from three laboratories demonstrating the ability of reducing agents such as CysNAc to inhibit the cytotoxicity of adaphostin (4–6) support the view that mitochondrial generation of ROS in the presence of adaphostin (Fig. 8*B*) plays a predominant role in the cytotoxicity.

These observations distinguish the action of adaphostin from those of a large class of anticancer drugs that are quinones. Previous studies have suggested that the cytotoxicity of these quinones is due to redox cycling between the quinone and semiquinone free radical, which generates ROS in the process (9). In contrast, our results provide little evidence for spontaneous oxidation of adaphostin in intact cells, but instead indicate that mitochondria play a role in the generation of ROS by

this antitumor hydroquinone. Whether complex III is a target of other hydroquinones and possibly even quinones remains to be determined.

Finally, because the involvement of complex III in adaphostin-induced increases in ROS levels suggested that the cytotoxic effects of this agent should not be limited to leukemia cells, we examined the effects of this agent in solid tumor cell lines. Drug-induced ROS elevations and sulfhydryl-sensitive killing were observed in HCT116 colon cancer cells, A549 lung cancer cells, and OVCAR5 ovarian cancer cells (Fig. 9) (data not shown). While this manuscript was under review, Long *et al.* (61) also reported that adaphostin induces ROS-mediated cytotoxicity in glioblastoma cells. Collectively, these observations suggest that adaphostin might be active against a wide variety of cancer cell types.

In summary, adaphostin is concentrated in mitochondria, where its ability to inhibit respiratory complex III appears to contribute to the intracellular generation of ROS. Moreover, this study has demonstrated adaphostin-induced oxidative damage of DNA in intact cells. Based on the unique mechanism of action of this agent and its demonstrated selectivity for leukemia cells *in vitro*, further study of this agent appears to be warranted.

Acknowledgments—The gifts of adaphostin and the corresponding quinone from Ven Narayanan, the advice of Gregory Gores, the technical assistance of Steve Bronk and the Mayo Clinic Flow Cytometry Shared Resource, and the secretarial assistance of Deb Strauss are gratefully acknowledged.

REFERENCES

1. Svingen, P. A., Tefferi, A., Kottke, T. J., Kaur, G., Narayanan, V. L., Sausville, E. A., and Kaufmann, S. H. (2000) *Clin. Cancer Res.* **6,** 237–249
2. Mow, B. M. F., Chandra, J., Svingen, P. A., Hallgren, C. G., Weisberg, E., Kottke, T. J., Narayanan, V. L., Litzow, M. R., Friggen, J. D., Sausville, E. A., Tefferi, A., and Kaufmann, S. H. (2002) *Blood* **99,** 664–671
3. Chandra, J., Tracy, J., Loegering, D., Flatten, K., Sverstovsek, S., Beran, M., Gorre, M. E., Estrov, Z., Donato, N., Talpaz, M., Sawyers, C., Bhalla, K., Karp, J. E., Sausville, E., and Kaufmann, S. H. (2006) *Blood* **107,** 2501–2506
4. Chandra, J., Hackbarth, J., Le, S., Loegering, D., Bone, N., Bruzek, L. M., Narayanan, V. L., Kay, N. E., Tefferi, A., Karp, J. E., Sausville, E. A., and Kaufmann, S. H. (2003) *Blood* **102,** 4512–4519
5. Shanafelt, T. D., Geyer, S. M., and Kay, N. E. (2004) *Blood* **103,** 1202–1210
6. Yu, C., Rahmani, M., Almenara, J., Sausville, E. A., Dent, P., and Grant, S. (2004) *Oncogene* **23,** 1364–1376
7. Laupeze, B., Amiot, L., Drenou, B., Bernard, M., Branger, B., Grosset, J. M., Lamy, T., Fauchet, R., and Fardel, O. (2002) *Br. J. Haematol.* **116,** 834–838
8. Walter, R. B., Raden, B. W., Hong, T. C., Flowers, D. A., Bernstein, I. D., and Linenberger, M. L. (2003) *Blood* **102,** 1466–1473
9. Powis, G. (1989) *Free Radic. Biol. Med.* **6,** 63–101
10. Cadenas, E. (1995) *Biochem. Pharmacol.* **49,** 127–140
11. Beall, H. D., and Winski, S. I. (2000) *Front. Biosci.* **5,** D639–D648
12. Gutierrez, P. L. (2000) *Free Radic. Biol. Med.* **29,** 263–275
13. Dawson, T. L., Gores, G. J., Nieminen, A. L., Herman, B., and Lemasters, J. J. (1993) *Am. J. Physiol.* **264,** C961–C967
14. Turrens, J. F. (2003) *J. Physiol.* (*Lond.*) **552,** 335–344
15. Balaban, R. S., Nemoto, S., and Finkel, T. (2005) *Cell* **120,** 483–495
16. Holmuhamedov, E. L., Jahangir, A., Bienengraeeber, M., Lewis, L. D., and Terzic, A. (2003) *Mitochondrion* **3,** 13–19
17. Kaufmann, S. H., Peereboom, D., Buckwalter, C. A., Svingen, P. A., Donehower, R. C., and Rowinsky, E. K. (1996) *J. Natl. Cancer Inst.* **88,** 734–741
18. Loegering, D., Arlander, S. A. H., Hackbarth, J., Vroman, B., Lieberman, H. B., Karnitz, L. M., and Kaufmann, S. H. (2004) *J. Biol. Chem.* **279,** 18641–18647
19. Okubo, T., Nagai, F., Ushiyama, K., and Kano, I. (1997) *Toxicol. Lett.* **90,** 11–18
20. Zhou, M., Diwu, Z., Panchuk-Voloshina, N., and Haugland, R. P. (1997) *Anal. Biochem.* **253,** 162–168
21. Pflaum, M., Will, O., and Epe, B. (1997) *Carcinogenesis* **18,** 2225–2231
22. Martins, L. M., Mesner, P. W., Kottke, T. J., Basi, G. S., Sinha, S., Tung, J. S., Svingen, P. A., Madden, B. J., Takahashi, A., McCormick, D. J., Earnshaw, W. C., and Kaufmann, S. H. (1997) *Blood* **90,** 4283–4296
23. Covey, J. M., Jaxel, C., Kohn, K. W., and Pommier, Y. (1989) *Cancer Res.* **49,** 5016–5022
24. Yang, J., Liu, X., Bhalla, K., Kim, C. N., Ibrado, A. M., Cai, J., Peng, T.-I., Jones, D. P., and Wang, X. (1997) *Science* **275,** 1129–1132
25. Qian, T., Nieminen, A. L., Herman, B., and Lemaster, J. J. (1997) *Am. J. Physiol.* **273,** C1783–C1792
26. Le, S. B., Holmuhamedov, E. L., Narayanan, V. L., Sausville, E. A., and Kaufmann, S. H. (2006) *Cell Death Differ.* **13,** 151–159
27. Holmuhamedov, E. L., Wang, L., and Terzic, A. (1999) *J. Physiol.* (*Lond.*) **519,** 347–360
28. Petronilli, V., Pietrobon, D., Zoratti, M., and Azzone, G. F. (1986) *Eur. J. Biochem.* **155,** 423–431
29. Kamo, N., Muratsugu, M., Hongoh, R., and Kobatake, Y. (1979) *J. Membr. Biol.* **49,** 105–121
30. Porteous, J. W., and Clark, B. (1965) *Biochem. J.* **96,** 159–171
31. Schwab, M. A., Kolker, S., van den Heuvel, L. P., Sauer, S., Wolf, N. I., Rating, D., Hoffmann, G. F., Smeitink, J. A., and Okun, J. G. (2005) *Clin. Chem.* **51,** 151–160
32. Trounce, I. A., Kim, Y. L., Jun, A. S., and Wallace, D. C. (1996) *Methods Enzymol.* **264,** 484–509
33. Pang, Y.-P., Perola, E., Xu, K., and Prenderast, F. G. (2001) *Journal Comput. Chem.* **22,** 1750–1771
34. Claassen, G. F., and Hann, S. R. (2000) *Proc. Natl. Acad. Sci. U. S. A.* **97,** 9498–9503
35. Frisch, M. J., Trucks, G. W., Schlegel, H. B., Gill, P. M. W., Hohnson, B. G., Robb, M. A., Raghavachari, K., Al-Laham, M. A., Zakrzewski, V. G., Ortiz, J. V., Foresman, J. B., Cioslowski, J., Stefanov, B. B., Nanayakkara, A., Challacombe, M., Peng, C. Y., Ayala, P. Y., Chen, W., Wong, M. W., Andres, J. L., Replogle, E. S., Gomperts, R., Martin, R. L., Fox, D. J., Binkley, J. S., Defrees, D. J., Baker, J., Stewart, J. P., Head-Gordon, M., Gonzales, C., and Pople, J. A. (1999) *Gaussian 03*, Gaussian, Inc., Wallingford, CT
36. Cornell, W. D., Cieplak, P., Bayly, C. I., Gould, I. R., Merz, K. M., Ferguson, D. M., Spellmeyer, D. C., Fox, T., Caldwell, J. W., and Killman, P. A. (1995) *J. Am. Chem. Soc.* **117,** 5179–5197
37. Pearlman, D. A., Case, D. A., Caldwell, J. W., Ross, W. S., Cheatham, T. E., III, DeBolt, S., Ferguson, D. M., Seibel, G. L., and Kollman, P. A. (1995) *Comput. Phys. Commun.* **91,** 1–41
38. Gao, X., Wen, X., Esser, L., Quinn, B., Yu, L., Yu, C.-A., and Xia, D. (2003) *Biochemistry* **42,** 9067–9080
39. Esser, L., Quinn, B., Li, Y.-F., Zhang, M., Elberry, M., Yu, L., Yu, C.-A., and Xia, D. (2004) *J. Mol. Biol.* **341,** 281–302
40. Pang, Y.-P. (2004) *Proteins Struct. Funct. Genet.* **57,** 747–757
41. Tchou, J., Kasai, H., Shibutani, S., Chung, M. H., Laval, J., Grollman, A. P., and Nishimura, S. (1991) *Proc. Natl. Acad. Sci. U. S. A.* **88,** 4690–4694
42. Sun, I. L., Sun, E. E., Crane, F. L., Morre, D. J., Lindgren, A., and Low, H. (1992) *Proc. Natl. Acad. Sci. U. S. A.* **89,** 11126–11130
43. Li, H., and Dryhurst, G. (1997) *J. Neurochem.* **69,** 1530–1541
44. Kowaltowski, A. J., Turin, J., Indig, G. L., and Vercesi, A. E. (1999) *J. Bioenerg. Biomembr.* **31,** 581–590
45. Xu, G. P., Dave, K. R., Moraes, C. T., Busto, R., Sick, T. J., Bradley, W. G., and Perez-Pinzon, M. A. (2001) *Neurosci. Lett.* **300,** 141–144
46. Rieske, J. S. (1976) *Biochim. Biophys. Acta* **456,** 195–247
47. Petrosillo, G., Ruggiero, F. M., and Paradies, G. (2003) *FASEB J.* **17,** 2202–2208
48. Turrens, J. F., and Boveris, A. (1980) *Biochem. J.* **191,** 421–427
49. Turrens, J. F., Freeman, B. A., Levitt, J. G., and Crapo, J. D. (1982) *Arch. Biochem. Biophys.* **217,** 401–410

50. Li, N., Ragheb, K., Lawler, G., Sturgis, J., Rajwa, B., Melendez, J. A., and Robinson, J. P. (2003) *J. Biol. Chem.* **278,** 8516–8525
51. Hose, C., Kaur, G., Sausville, E. A., and Monks, A. (2005) *Clin. Cancer Res.* **11,** 6370–6381
52. Sattler, M., Verma, S., Shrikhande, G., Byrne, C. H., Pride, Y. B., Winkler, T., Greenfield, E. A., Salgia, R., and Griffin, J. D. (2000) *J. Biol. Chem.* **275,** 24273–24278
53. Potter, V. R., and Reif, A. E. (1952) *J. Biol. Chem.* **194,** 287–297
54. von Jagow, G., and Link, T. A. (1986) *Methods Enzymol.* **126,** 253–271
55. Wallace, K. B., and Starkov, A. A. (2000) *Annu. Rev. Pharmacol. Toxicol.* **40,** 353–388
56. Hamilton, P. B., Carroll, F. I., Rutledge, J. H., Mason, J. E., Harris, B. S., Fenske, C. S., and Wall, M. E. (1969) *Appl. Microbiol.* **17,** 102–105
57. Summerhayes, I. C., Lampidis, T. J., Bernal, S. D., Nadakavukaren, J. J., Nadakavukaren, K. K., Shepherd, E. L., and Chen, L. B. (1982) *Proc. Natl. Acad. Sci. U. S. A.* **79,** 5292–5296
58. Nadakavukaren, K. K., Nadakavukaren, J. J., and Chen, L. B. (1985) *Cancer Res.* **45,** 6093–6099
59. Lampidis, T. J., Hasin, Y., Weiss, M. J., and Chen, L. B. (1985) *Biomed. Pharmacother.* **39,** 220–226
60. Weiss, M. J., Wong, J. R., Ha, C. S., Bleday, R., Salem, R. R., Steele, G. D., Jr., and Chen, L. B. (1987) *Proc. Natl. Acad. Sci. U. S. A.* **84,** 5444–5448
61. Long, J., Manchandia, T., Ban, K., Gao, S., Miller, C., and Chandra, J. (2007) *Cancer Chemother. Pharmacol.* **59,** 527–535